Multi-scale modeling and diffraction-based characterization of elastic behaviour of human enamel

Tan Sui[1,*], Michael A. Sandholzer[2], Nikolaos Baimpas[1], Igor Dolbnya[3], Gabriel Landini[2], Alexander M. Korsunsky[1]

[1] Department of Engineering Science, University of Oxford, Parks Road, Oxford OX1 3PJ, United Kingdom
[2] School of Dentistry, College of Medical and Dental Sciences, University of Birmingham, St Chad's Queensway, Birmingham B4 6NN, United Kingdom
[3] Diamond Light Source, Harwell Oxford Campus, Didcot OX11 0DE, United Kingdom

* Corresponding author: tan.sui@eng.ox.ac.uk

Abstract The relationship between the ultrastructure of human enamel and its mechanical behaviour is studied in this paper. Two synchrotron X-ray diffraction techniques, wide and small angle X-ray scattering (WAXS/SAXS) were used in combination to obtain multi-scale quantitative information about the response of human enamel to *in situ* uniaxial compressive loading. The interpretation of WAXS data gives elastic lattice strains within the hydroxyapatite (HAp) crystals, the stiff reinforcing phase in human enamel. The apparent modulus was determined linking the external load and the internal HAp strain. SAXS interpretation, allows the quantification of the nano-scale HAp crystallite distribution within human enamel. A multi-scale Eshelby equivalent inclusion model of the enamel was proposed that represents the hierarchical mineralized tissue as a two-level composite: micro-level model with rod embedded in the homogenised enamel material, and nano-level model with HAp crystallites embedded in the rod. Satisfactory agreement was achieved between model and experiment, suggesting that the new multi-scale approach accurately reflects the structure and mechanics of human enamel, and may help guide new biomimetic designs.

Keywords Enamel, WAXS/SAXS, Eshelby model, Mechanical properties

1. Introduction

Enamel, a highly mineralized substance, is a hard and brittle material that covers the crown portion of teeth. It is predominately composed of inorganic hydroxyapatite (HAp) crystals and organic collagen [1]. While at the macro-scale the enamel can be thought of as a continuum, at the microstructural level some notable features are present, in particular, aligned long prisms (or rods) with a keyhole-shaped cross-section, and with the top oriented toward the crown of the tooth [2]. Further, at the nano-scale level, needle-like HAp crystals are found with several tens of nanometers in thickness [3].

Understanding the effects of microstructural features of enamel on the performance of human teeth requires the understanding of how the mechanical properties are related to the complex hierarchical structure. Over half a century, studies have been conducted on the macro-scale mechanical properties of enamel [4]. While an increasing number of publications describe microstructural effects [5], relatively few studies have focused on the influence of the nano-scale structure [6]. There appears to be a demand for further investigation across the scales using advanced techniques and models to establish a solid basis to understand the hierarchical structure-property relationship.

One suitable method to study this is small angle X-ray scattering (SAXS), an advanced non-destructive technique used to reveal information about nano-scale structure and orientation in crystalline and amorphous materials [7]. Another X-ray technique, wide angle X-ray scattering (WAXS), is used to study crystal lattices and their deformation behaviour, e.g. the elastic properties of composites [8,9]. WAXS has been applied only recently to the study of mineralized biological composites, such as bones and bovine teeth [10-13], but few studies have been devoted to study human enamel [14]. Therefore, for the present study a combined SAXS/WAXS setup with *in situ* compressive loading of human enamel samples was selected. It is hoped that the results obtained

here will be helpful to understand the internal architecture and hierarchical properties of human dental tissues.

Quite a few models of composites have been proposed to describe the interaction of different phases, including bounding principles of Voigt and Reuss, as well as Jones and BW models [15,16]. One widely accepted model, also used in this study, is the Eshelby inclusion model, often used to describe the structure-property relationship of materials like composites [17,18]. Recently, it has been applied in the research of dentine [19,20], and has been proven to be useful to predict the elastic response of dentine. However, this Eshelby approach has not been used to describe human enamel.

In this paper, the elastic lattice strain, orientation and degree of alignment of HAp crystals within a human enamel sample under compressive loading were measured by the combined *in situ* synchrotron X-ray techniques (WAXS and SAXS). The multi-scale Eshelby model was developed to reflect the hierarchical structure of enamel, and to predict the elastic response to mechanical loading. The model was validated by comparison with experimental data.

2. Method and Materials

2.1. Sample preparation

A freshly extracted sound human third molar (ethical approval obtained from the National Research Ethics Committee; NHS-REC reference 09.H0405.33/Consortium R&D No.1465) was washed and mechanically cleaned in distilled water to eliminate residues and kept in a -20°C freezer for a maximum of 14 days before the experiment. The tooth was rehydrated using distilled water and 2mm thick enamel disks were cut just below the enamel-cement line using a low speed diamond saw (Isomet Buehler Ltd., Lake Bluff, Illinois, USA). The disks were further cut into smaller bars and polished using a series of polishing papers to produce a 2×2×2mm cube of enamel. The sample was kept for 5 days in distilled water in a commercial fridge at 4°C until the experiment was undertaken.

2.2. In-situ scattering measurements

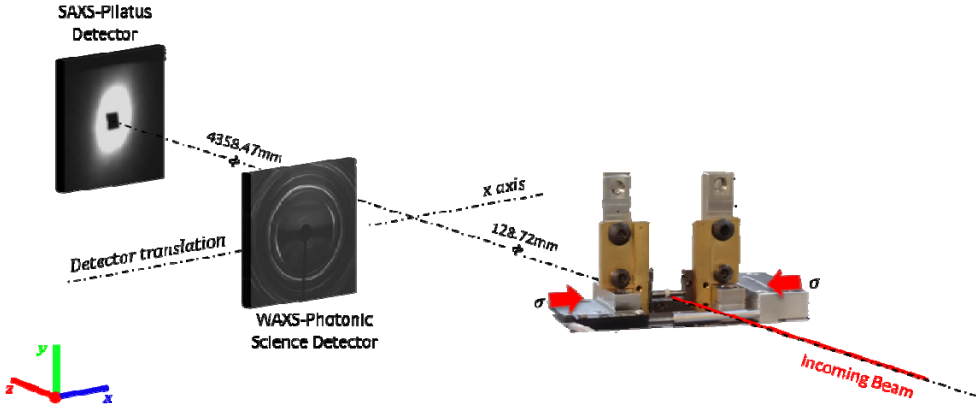

Figure 1. In situ loading of enamel under simultaneous WAXS/SAXS experimental set-up

The experiment was performed on the B16 beamline at Diamond Light Source (DLS, Oxford, UK). A schematic diagram of the experimental set-up is shown in Fig. 1. The cubic sample of human enamel was slowly deformed along x-direction in the laboratory coordinate system (Fig. 1) under compressive loading at a displacement rate of 0.2 mm/min until failure, using a remotely operated and monitored compression rig (Deben, Suffolk, UK) with a 5KN calibrated load cell.

The monochromatic X-ray beam at the photon energy of 17.99keV was used and collimated to the spot size of 0.5× 0.5mm^2. The beam was incident at the sample perpendicular to its loading direction. Two separate WAXS and SAXS detectors were alternately setup to collect the patterns at consecutive loading increments downstream of the beam. WAXS patterns were recorded using a Photonic Science Image Star 9000 detector (Photonic Science Ltd., UK) with a sample-to-camera distance of 128.72mm. Further downstream, a Pilatus 300K detector (Dectris, Baden, Switzerland) was positioned at a distance of 4358.47mm to collect SAXS patterns. In order to record both WAXS and SAXS patterns at each scanning location, the WAXS detector was translated laterally to expose the SAXS detector after each WAXS exposure. A lightly compacted disk of standard silicon powder and a dry chicken collagen sample inserted close to the sample position were used as calibration standards, and to determine the sample-to-detector distance to good precision.

2.3. Scattering data analysis

2.3.1. WAXS data analysis

WAXS data can be interpreted in terms of the shift of the diffraction peak obtained from a cluster of HAp crystals, so that the average micro-strain (lattice strain) in the crystals can be deduced [8,9]. The typical WAXS pattern of HAp is shown in Fig. 2 (only the (002) peak is selected for interpretation). The apparent elastic lattice strain of the HAp phase was computed by observing the changes in the interplanar spacing between the lattice planes [21]:

$$\varepsilon = \frac{d_{002} - d_{002}^0}{d_{002}^0} \tag{1}$$

where d_{002} is the deformed *d*-spacing and d_{002}^0 is the reference strain-free value. In detail, 2D diffraction images were firstly pre-processed using Fit2D [22]. The (002) peak of interest from each pattern was “caked” (i.e. binned in the radial-azimuthal coordinates) within a range of 20^o in the loading direction (Fig. 2a). Subsequently the 1D radial plot of intensity within each sector was fitted with Gaussian to obtain the peak centre position. As the load increase, the peak centre position shift with respect to the strain-free reference point allowed the calculation of HAp elastic lattice strain. In addition, the structural orientation angle was determined from the strain-free sample by azimuthal-radial “caking” of the (002) peak over the entire range of 360^o, and fitting the azimuthal centre position of the pronounced peaks [23].

2.3.2. SAXS data analysis

For SAXS data analysis, the pattern from the strain-free sample was taken as reference. Due to the dense distribution of crystals in enamel, the electron density changes that occur in the gaps between crystalline particles gives rise to the scattering signal [24]. It is also understood that the orientation of the gaps between rods roughly coincides with the orientation of the crystals within the rod [19]. Thus, the information from gap scattering can be used to deduce the orientation and degree of alignment (percentage of aligned particles) of HAp crystals. To quantify it, the 2D SAXS patterns were processed by integrating over the entire relevant range of scattering vector *a*, resulting in a function $I(\varphi)$ of the azimuthal angle φ [25,26]. The predominant orientation φ_0 of the mineral crystals is determined by the position of the two peaks in the plot of $I(\varphi)$. Further, the degree of alignment ρ can be calculated by the ratio of the two areas under the curve of $I(\varphi)$:

$$\rho = \frac{A_{oriented}}{A_{total}} \tag{2}$$

where A_{total} is the total area below the curve, and $A_{oriented}$ refers to the area above the constant background level $A_{umoriented}$. Thus, the value of ρ ranges from 0 to 1, with $\rho = 0$ indicating no predominant orientation within the plane of the section, while $\rho = 1$ indicates a perfect alignment of all crystals [25,26].

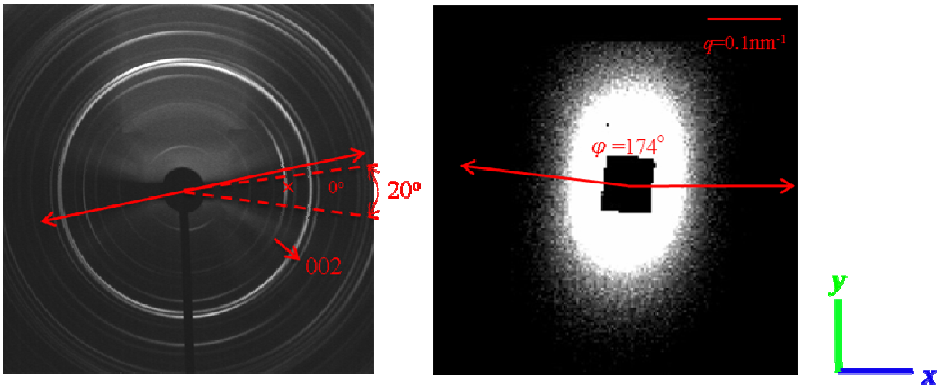

Figure 2. Representative WAXS and SAXS patterns of enamel

3. Model formulation

Human enamel has a hierarchical two-level composite structure, where the first level is represented by the keyhole-like rod and the second level by the bunch of HAp crystals within one rod [27]. Fig. 3a shows the keyhole-like microstructure of enamel, modified from Habelitz [28], and demonstrates how the HAp crystals are distributed within the rod in 3D. Fig. 3b-d provide schematic illustration of the geometric model derived from the enamel structure, where the first level regards the whole enamel sample as composed of aligned rods within a collagen matrix phase (Fig. 3b), and the second level considers the rod as a composite in detail, consisting of partially aligned HAp crystals and a collagen matrix. Both levels are non-dilute systems with a number of inhomogeneous inclusions. For simplicity, both rod and HAp crystals are assumed to be of needle shape (Fig. 3b-d).

3.1. First level model: multiple aligned rod inclusions within enamel

The purpose of the first-level model is to establish the relationship between the externally measured stress σ^A and the stress in the rod inclusions $\sigma^{inclusion} = \sigma^{rod}$. According to the Eshelby model derivation [29], the stress in the inclusion can be expressed as

$$\sigma^{inclusion1} = \left\{T - (1-f_1)\left\{(C_{matrix1} - C_{rod})\left[S_1 - f_1(S_1 - I)\right] - C_{matrix1}\right\}^{-1}(C_{matrix1} - C_{rod})T^{-T}C_{matrix1}^{-1}\right\}\sigma^A$$

$$\text{or, simplified } \sigma^{inclusion1} = K_1\sigma^A \tag{3}$$

where f_1 is the volume fraction of rod inclusion, S_1 the Eshelby tensor for a cylinder corresponding to the rod shape, $C_{matrix1}$ and C_{rod} are the stiffness of collagen matrix and rod, respectively, and T is the tensor transformation (rotation) matrix that depends on the Euler angles giving the orientation of the rods with respect to the fixed laboratory system. In the present model this was fixed, as it was

assumed that the rods were all aligned with the loading direction.

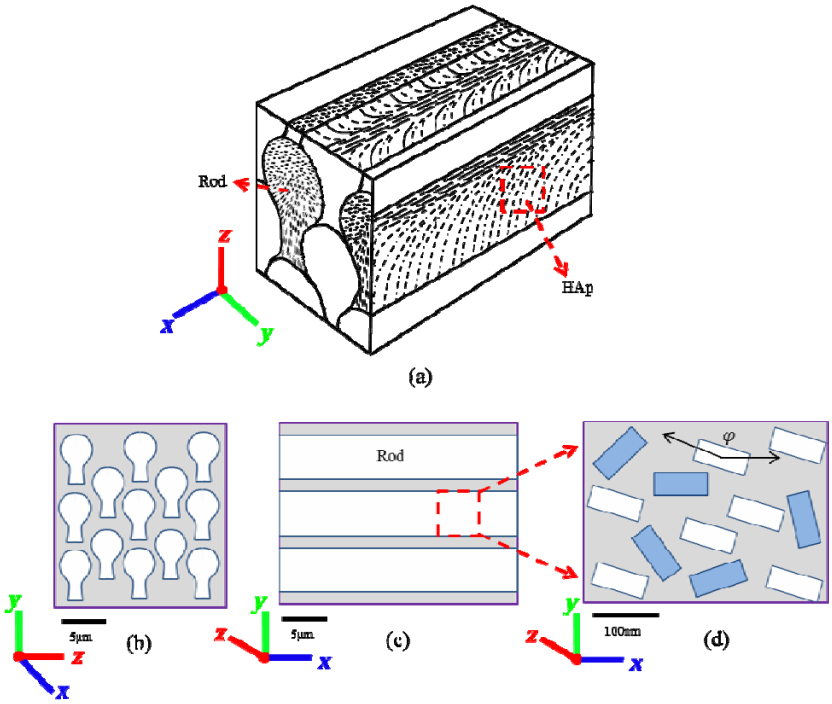

Figure 3. Schematic diagrams of hieratical enamel structure and multi-scale Eshelby model.

To determine the stress within the inclusion, knowledge of the rod stiffness matrix is required. The rod is regarded as a composite consisting of the same volume fraction of collagen and mineral crystals as the whole enamel. The stiffness of the rod C_{rod} can thus be determined and is given as:

$$C_{rod} = \left\{ C_{matrix2}^{-1} - f_2 \left\{ \left(\langle C \rangle_{HAp} - C_{matrix\_2} \right) \left[\langle S_2 \rangle - f_2 \left(\langle S_2 \rangle - I \right) \right] + C_{matrix2} \right\}^{-1} \left(\langle C \rangle_{HAp} - C_{matrix2} \right) C_{matrix2}^{-1} \right\}^{-1} \quad (4)$$

3.2. Second level model: HAp inclusion within one rod

The purpose of the second-level model is to establish the relationship between the external stress and the average strain in the HAp crystals in a rod: $\langle \varepsilon \rangle^{HAp}$ ($\sigma^{inclusion1} = K \langle \varepsilon \rangle^{HAp}$). Here the stress within the rod inclusion $\sigma^{inclusion1}$ found from the first-level model serves as the external stress in the second-level model. The overall stiffness of the rod C_{rod} is required to link the average strain in the HAp crystals with the external stress obtained in the first-level model. A single HAp crystal can be regarded as a single inhomogeneity with needle-like shape, and thus the corresponding Eshelby tensor S_2 should again be that for the cylinder. The alignment of HAp crystals within the rod is also partial, so that the real value of the apparent stiffness *K* is given by a combination of the values for two separate cases, namely, that of fully random distribution, and perfect alignment.

3.2.1 Multiple perfectly aligned HAp crystals

Supposing the alignment direction of HAp crystals is described by the transformation matrix *T*, the measured crystal strain corresponds to the mean strain value for all the crystals within the considered gauge volume. The relationship between the average HAp strain and the external load (rod stress from the first-level model) can be established as follows:

$$\langle \varepsilon \rangle_{aligned}^{HAp} = \left\{ \left\{ \left(I - C_{matrix2}{}^{-1} \langle C \rangle_{HAp} \right)^{-1} \left[\langle S_2 \rangle - f_2 (\langle S_2 \rangle - I) \right]^{-1} - I \right\}^{-1} T^{-T} + T^{-T} \right\} C_{matrix2}{}^{-1} \sigma^{inclusion1}$$

$$\text{or, simplified} \quad \sigma^{inclusion1} = K_{aligned} \langle \varepsilon \rangle_{aligned}^{HAp} \tag{5}$$

where $\langle C \rangle_{HAp}$ and $\langle S_2 \rangle$ are the average elastic stiffness tensor and Eshelby tensor of HAp crystals within gauge volume [30], f_2 the volume fraction of HAp with respect to the entire rod, and $C_{matrix2}$ is the stiffness tensor of collagen. Since all the crystals are perfectly aligned, the average value of $\langle C \rangle_{HAp}$ and $\langle S_2 \rangle$ can be represented by the single crystal values $\langle C \rangle_{HAp} = C_{HAp}, \langle S_2 \rangle = S_2$. Note that different orientation angles would lead to different values of $\langle \varepsilon \rangle_{aligned}^{HAp}$.

3.2.2 Multiple randomly distributed HAp crystals

The relationship between the average HAp lattice strain and rod stress is independent of the transformation matrix in Eq. 5 in the case of an isotropic cluster with randomly distributed crystals. The relationship becomes

$$\langle \varepsilon \rangle_{random}^{HAp} = \left\{ \left\{ \left(I - C_{matrix2}{}^{-1} \langle C \rangle_{HAp} \right)^{-1} \left[\langle S_2 \rangle - f_2 (\langle S_2 \rangle - I) \right]^{-1} - I \right\}^{-1} + I \right\} C_{matrix2}{}^{-1} \sigma^{inclusion1}$$

$$\text{or, simplified} \quad \sigma^{inclusion1} = K_{random} \langle \varepsilon \rangle_{random}^{HAp} \tag{6}$$

Note that in contrast with the case of perfectly aligned crystals, the average value of $\langle S_2 \rangle$ no longer equals the single crystal value S_2. Instead, it must be obtained by the volume average over all the crystals.

3.2.3 Multiple HAp inclusions with partial orientation

For the partially aligned HAp distribution (Fig. 3d), $K_{partial\_aligned}^{HAp}$ is given by the mixtures between K_{random} and $K_{aligned}$:

$$K_{partial\_aligned}^{HAp} = (1 - f_{aligned}) K_{random} + f_{aligned} K_{aligned} \tag{7}$$

where $f_{aligned}$ is the volume fraction of the aligned crystals with respect to all HAp crystals, i.e. the degree of alignment of crystals revealed by SAXS. Thus, the relationship between external stress (in rod) and average internal HAp lattice strain becomes

$$\sigma^{inclusion1} = K_{partial\_aligned}^{HAp} \langle \varepsilon \rangle^{HAp} \tag{8}$$

Further, the relationship between HAp strain and the externally applied stress can be established by combining Eq. 3 and Eq.8.

$$\sigma^{A} = K_1^{-1} \sigma^{inclusion1} = K_1^{-1} K_{partial\_aligned}^{HAp} \langle \varepsilon \rangle^{HAp} = K \langle \varepsilon \rangle^{HAp} \tag{9}$$

4. Experimental results and model evaluation

4.1. Nano-scale HAp distribution and the mechanical response of enamel

The apparent radial shifts of the (002) peak centre position obtained from the WAXS pattern (Fig. 2a) were measured under compressive loading applied on the longitudinal direction with respect to

the rods. Fig. 4a shows the experimental results of the applied stress vs. HAp lattice strain, indicating the expected linear relationship. The ratio of the stress and the average HAp lattice strain gives the apparent modulus [31]. The preferential orientation of HAp crystals obtained by WAXS pattern analysis is shown to be roughly perpendicular to the arc, while that obtained by SAXS pattern is shown to be roughly along the short axis of the elliptical SAXS pattern (Fig. 2). The detailed values from experiment and model are listed in Table 1.

4.2. Evaluation and testing of multi-scale Eshelby model

In the model, the material properties and other parameters were derived from the literature, and refined by fitting with the experimental data. The average mineral concentration (HAp volume fraction) has been reported to be ~95% in each level of enamel, so that the overall volume fraction of HAp could be close to 85%, which is consistent with [6]. In general, Young's modulus of 1GPa for collagen is found in the literature, without taking into account the viscoelasticity or viscoplasticity [19,20]. Polycrystalline HAp is considered to be transversely isotropic with five independent elastic constants [32]. To describe the shape of the rod and of the HAp crystallites for each level, the Eshelby tensor for the cylinder was used. It was assumed that the lengths of ellisptical axes a_1 and a_2 within the transverse cross-section were the same, a_1/a_2=1). The apparent modulus K was calculated based on the different preferred orientation angles of the HAp crystals obtained by both SAXS and WAXS. All the parameters refined to obtain the best fit are listed in Table 1. A comparison of the experimental results and the model evaluation is plotted in Fig. 4. Good agreement is observed.

Table 1 Experimental results from SAXS/WAXS, and the refined structural parameters of the enamel used in the two-level Eshelby model

Parameter	**Enamel**
Orientation (from SAXS)	174°
Orientation (from WAXS)	14°
Degree of alignment	0.6
K_exp.	124.3 GPa
$f_1 = f_2$	96%
C_{matix1}	E_m=1GPa, v_m=0.3
C_{matix2}	E_m=1GPa, v_m=0.3
C_{HAp}	E_{xx}=140GPa, G_{xy}= G_{xz}=39.6GPa v_{xy}= v_{xz} =0.3, v_{yz}=0.2 E_{yy}= E_{zz}=114.3GPa
$S_{cylinder1} = S_{cylinder2}$	$a_1 / a_2 = 1$
K_model (from SAXS)	122.9 GPa
K_model (from WAXS)	120.4 Gpa

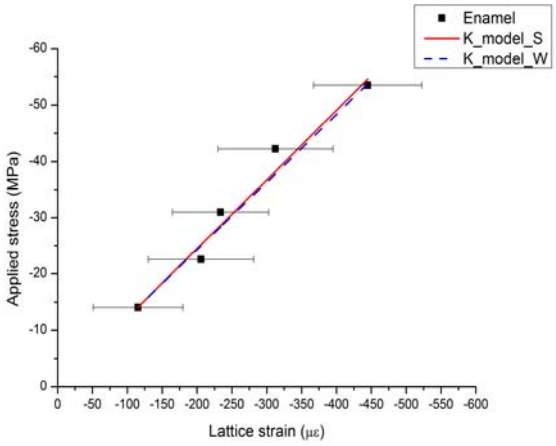

Figure 4. Comparison of the experimental data (markers) and modeling results for applied compressive stress vs. elastic lattice strain for HAp crystals.

5. Discussion & Conclusion

The agreement of the apparent modulus K results calculated using the HAp preferred orientation angles determined by SAXS and WAXS suggests that the SAXS patterns arising from gap scattering can be used to deduce the HAp orientation distribution, i.e. the gaps are almost parallel to HAp crystals inside the rod. Further validation can be demonstrated by examining in more detail the effect of crystal orientation on the apparent modulus. A 3D model of perfectly aligned crystals inside a rod is established (Fig. 5a) with the angle φ describing the rotation of the alignment direction around the global z axis. When all HAp crystals are aligned along the global x-direction, φ equals to 0°. By changing the perfect alignment direction (changing the transformation matrix in Eq. 5), the variation of $K_{aligned}$ obtained in the loading direction can be calculated (Fig. 5b). From Fig. 5b, the corresponding results using the real orientation angles found in the experiment (174° from SAXS and 14° from WAXS) are found to be $K_{aligned\_SAXS} =$ 133.19GPa and $K_{aligned\_WAXS} =$ 128.25 GPa, i.e. closely similar values. Meanwhile, due to the high degree of alignment of HAp crystals in the enamel, the value of the overall apparent modulus $K^{HAp}_{partial\_aligned}$ lies close to the value $K_{aligned}$. The enamel displays strong microscopic elastic anisotropy. It is interesting to note that the stiffest orientation is, as expected, around 0° with respect to the loading direction. However, the most compliant orientation observed is not at 90°, i.e. perpendicular to the loading direction, but rather around 50° or 130°.

In this study, the longitudinal apparent Young's modulus of human enamel was measured during in situ elastic compression by the combination of synchrotron WAXS and SAXS for the first time. This provides access to the information on both the structural and mechanical aspects of the sample and allows us to make further progress compared to previous studies that only used WAXS [11,14]. A multi-scale Eshelby inclusion model was established to estimate the elastic material properties of the enamel in terms of its constituents, considering it as a two-level composite. Good agreement with the experimental data was obtained, indicating an improvement of the earlier proposed composite model [15,16] The model offers a powerful tool for the evaluation of the apparent modulus of enamel-like composites, and helps understand the relationship between the external load

and the internal HAp strain. It also helps understanding of the mechanical properties of hierarchical biomaterials.

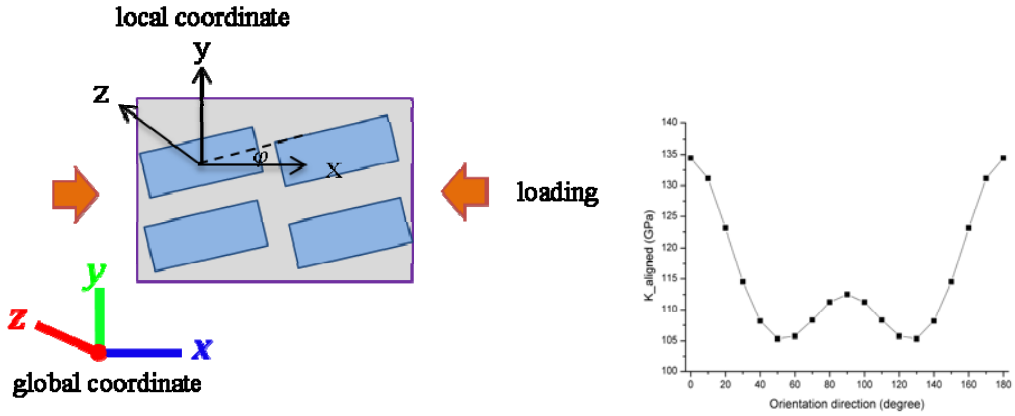

Figure 5. (a) A simple 3D example of aligned HAp crystals (alignment angle φ=0° is shown). (b) $K_{aligned}$ variation with respect to the alignment angle (0°-180°).

Acknowledgements

Diamond Light Source is acknowledged for the provision of beamtime at Test Beamline B16 under allocations MT7807 and MT7989. AMK wishes to acknowledge EPSRC support through grants EP/H003215/1 and EP/I020691/1, and the use of facilities at the Research Complex at Harwell.

References

[1] F.A. Siang, S. Mahnaz, V.S. Michael, *et al*. Comparison of mechanical behaviours of enamel rod and interrod regions in enamel. J Mater Res., 27 (2012) 448-456.
[2] G.A. Macho, Y. Jiang, I.R. Spears. Enamel microstructure—a truly three-dimensional structure. J Hum Evol., 45 (2003) 81-90.
[3] B. Kerebel, G. Daculsi, L.M. Kerebel. Ultrastructural studies of enamel crystallites. J Dent Res. 57 (1979) 306-312.
[4] L.H. He. Mechanical behavior of human enamel and the relationship to its structural and compositional characteristics. phd thesis, 2008.
[5] T. Nakamura, C. Lu, C.S. Korach, Mechanical Properties of Tooth Enamel: Microstructural Modeling and Characterization, Conference Proceedings of the Society for Experimental Mechanics Series, 2011(9999) 171-179.
[6] S. Bechtle, H. Özcoban, E.T. Lilleodden, *et al*. Hierarchical flexural strength of enamel: transition from brittle to damage-tolerant behavior. J.R. Soc. Interface, 9 (2012) 1265-1274.
[7] P. Fratzl, S. Schreiber, K. Klaushofer. Bone mineralization as studied by small-angle x-ray scattering. Connect Tissue Res., 34 (1996) 247-254.
[8] M.L. Young, J.D. Almer, M.R. Daymond, *et al*. Load partitioning between ferrite and cementite during elasto-plastic deformation of an ultrahigh-carbon steel. Acta Mater, 55 (2007) 1999–2011.
[9] M.L. Young, J. DeFouw, J.D. Almer, *et al*. Load partitioning during compressive loading of a Mg/MgB2 composite. Acta Mater, 55 (2007) 3467–3478.
[10] A.C. Deymier-Black, J.D. Almer, S.R. Stock, *et al*. Synchrotron X-ray diffraction study of load partitioning during elastic deformation of bovine dentin. Acta Biomater, 6 (2010) 2172–2180.
[11] J.D. Almer, S.R. Stock. High energy X-ray scattering quantification of in situ-loading-related strain gradients spanning the dentin enamel junction (DEJ) in bovine tooth specimens. J Biomech., 43 (2010) 2294–2300.
[12] A. Singhal, J.D. Almer, D.C. Dunand. Variability in the nanoscale deformation of

hydroxyapatite during compressive loading in bovine bone. Acta Biomater., 8 (2012) 2747–2758.
[13] J.D. Almer, S.R. Stock. Internal strains and stresses measured in cortical bone via high-energy X-ray diffraction. J Struct Biol., 152 (2005) 14–27.
[14] K. Fujisaki, M. Todoh, A. Niida, *et al*. Orientation and deformation of mineral crystals in tooth surfaces. J Mech Behav Biomed Mater, 10 (2012), 176-182.
[15] R.M. Jones. Mechanics of Composite Materials, Second edition. Taylor&Francis, Inc., Philadelphia, PA, 1999.
[16] B. Bar-On, H.D. Wagner. Elastic modulus of hard tissues. J. Biomech. 45(2012a), 672–678.
[17] P.J. Withers, W.M. Stobbs, O.B. Pedersen. The application of the Eshelby method of internal stress determination to short fibre metal matrix composites. Acta Metallurgica. 37 (1989) 3061-3084.
[18] Y. Takao, M. Taya. The effect of variable fiber aspect ratio on the stiffness and thermal-expansion coefficients of a short fiber composite. J Compos Mater., 21 (1987) 140-156.
[19] Q.H. Qin, M.V. Swain. A micro-mechanics model of dentine mechanical properties. Biomaterials, 25 (2004) 5081-5090.
[20] B. Huo. An inhomogeneous and anisotropic constitutive model of human dentin. J Biomech, 38 (2005) 587-594.
[21] A.M. Korsunsky, N. Baimpas, X. Song, *et al*. Strain tomography of polycrystalline zirconia dental prostheses by synchrotron X-ray diffraction. Acta Mater, 59 (2011) 2501-2513.
[22] A.P. Hammersley. "FIT2D: An Introduction and Overview". ESRF Internal Report1997.
[23] M. Al-Jawad, A. Steuwer, S.H. Kilcoyne, 2D mapping of texture and lattice parameters of dental enamel, Biomaterials. 28 (2007) :2908-2914.
[24] T. Tanaka, N. Yagi, T. Oht, *et al*. Evaluation of the distribution and orientation of remineralized enamel crystallites in subsurface lesions by X-Ray diffraction. Caries Res, 44 (2010) 253-259
[25] W. Tesch, T. Vandenbos, P. Roschgr, *et al*. Orientation of mineral crystallites and mineral density during skeletal development in mice deficient in tissue nonspecific alkaline phosphatase. J Bone Miner Res, 18 (2003) 117-125.
[26] W. Tesch, N. Eidelman, P. Roschger, *et al*. Graded microstructure and mechanical properties of human crown dentin. Calcified Tissue Int., 69 (2001) 147-57.
[27] A. Nanci. Ten Cate's Oral Histology: Development, Structure and Function. MosbyInc, St. Louis, Missouri, 2003.
[28] S. Habelitz, S.J. Marshall, G.W. Marshall Jr, *et al*. Mechanical properties of human dental enamel on the nanometre scale. Arch Oral Biol., 46 (2001) 173-183.
[29] T.W. Clyne, P.J. Withers. An introduction to metal matrix composites. First paperback edition 1995. ed. Cambridge: Cambridge University Press; 1993.
[30] T.W. Chou, C.T. Sun. Nanocomposites. In: Hyer M, W, editor.: DEStech Inc; 2012.
[31] J.M. Powers, J.W. Farah. Apparent Modulus of Elasticity of Dental Amalgams. J Dent Res, 54 (1975) 902.
[32] A. Öchsner, W. Ahmed, Biomechanics of Hard Tissues, John Wiley & Sons, 2011